How upgoing and downgoing energy fluxes contribute to the establishment of lamb waves in an immersed elastic plate

Eric Ducasse, Marc Deschamps

ACOUSTICS 2012

How upgoing and downgoing energy fluxes contribute to the establishment of lamb waves in an immersed elastic plate

E. Ducasse and M. Deschamps

Institut de Mécanique et d'Ingénierie de Bordeaux (I2M), UMR CNRS 5295, Arts et Métiers ParisTech, Université de Bordeaux, 351 cours de la Libération, 33405 Talence, France
e.ducasse@i2m.u-bordeaux1.fr

Ultrasonic guided waves in an anisotropic elastic plate immersed in a fluid can be considered as the result of successive reflections from the plate walls. Inhomogeneous (surface) waves are involved in the problem if the incidence angle is greater than the first critical angle.
In this latter case, the energy is transmitted from one side to the other by the coupling of two inhomogeneous waves with conjugate wavenumbers and same kind of polarization, whereas each of these latter inhomogeneous waves does not transfer energy through the plate.
Thus, *nonstandard upgoing and downgoing waves* are defined such that, firstly, their power fluxes are upgoing and downgoing, respectively, and, lastly, their interaction energy is zero.
In this light, an interesting physical phenomenon is described for one specific pair "*angle of incidence/frequency*": the quasi-energy brought by the incident harmonic plane wave crosses the plate without any conversion to reflected waves either at the first interface or at the second interface. In this zone, there is a perfect impedance matching between the fluid and the plate. This case is remarkable because a full energy transmission from one side to the other generally corresponds to a Lamb wave, usually considered as the result of interferences of multiple reflections.

1 Introduction

On the basis of a recent work [2], which proposes a method to insure the convergence of the series resulting from the multiple reflections/refractions by an immersed plate, the construction of Lamb waves is presented as constructive interferences for any angles of incidence, *i.e.* beyond or before each critical angle. Up to now, this explanation was restricted to the case of angles of incidence less than the smallest critical angle. This work constitutes, from this point of view, a generalization. Beyond this improvement, an interesting phenomenon has been observed close to the Rayleigh angle for an aluminium plate immersed in water. At this incidence angle, the incident wave in the upper fluid is totally transmitted to the lower fluid, without any multiple reflection/refraction -in the plate- of the waves defined in the new wave basis. The plate seems to be really transparent, in a sense that no energy stays in the guide.

2 Theoretical background

2.1 Acoustic fields in the fluid

The plate is insonified by an incident time-harmonic plane wave of incidence angle θ and angular frequency ω. Due to the Snell-Descartes law related to the reflection/refraction of harmonic plane waves, the factor $\exp[\mathrm{i}\,\omega\,(\tau - s_x\,x)]$, containing the dependence with respect to time τ and abscissa x, $s_x = \sin(\theta)\,/\,c$ being the slowness in the x-direction and c the sound velocity in the fluid, necessarily appears in all expressions of acoustic fields (see Fig. 1). Hence, the latter factor will be then omitted below.

The incident acoustic wave is characterized by the acoustic pressure:

$$p_{\text{inc}}(z) = a_{\text{inc}} \sqrt{\frac{2\,s_z}{\rho}}\,\exp[\mathrm{i}\,s_z\,(z-H)]\,,\ z > h\,, \qquad (1)$$

$s_z = \cos(\theta)\,/\,c$ denoting the slowness in the z-direction, ρ the fluid density, $2h$ the thickness of the plate, $z = \omega z$ and $H = \omega h$ frequency-position products. The coefficient $\sqrt{2\,s_z\,/\,\rho}$ is due to normalization with respect to the mean power flux in the z-direction, that is, the mean power flux is negative and equal to $-\,|\,a_{\text{inc}}\,|^2$.

Thus, the reflected (upgoing) field is given by:

$$p_{\text{ref}}(z) = a_{\text{ref}} \sqrt{\frac{2\,s_z}{\rho}}\,\exp[-\mathrm{i}\,s_z\,(z-H)]\ ,\ z > h\,, \qquad (2)$$

such that its mean power flux in the z-direction is positive and equal to $|\,a_{\text{ref}}\,|^2$.

The transmitted (downgoing) field in the fluid below the plate is characterized by:

$$p_{\text{tr}}(z) = a_{\text{tr}} \sqrt{\frac{2\,s_z}{\rho}}\,\exp[\mathrm{i}\,s_z\,(z+H)]\ ,\ z < -h\,. \qquad (3)$$

such that its mean power flux in the z-direction is negative and equal to $-\,|\,a_{\text{tr}}\,|^2$.

Due to the linearity of the problem, the reflection and transmission coefficients r and t are defined such that $a_{\text{ref}} = r\,a_{\text{inc}}$ and $a_{\text{tr}} = t\,a_{\text{inc}}$. Energy conservation implies that $|\,r\,|^2 + |t\,|^2 = 1$.

2.2 Elastodynamic field in the plate

2.2.1 Standard decomposition

By using Stroh sextic formalism (*e.g.*, [6, 3, 1, 7, 5]), the vibrational state of the elastic anisotropic plate is described by the following six-dimensional vector:

$$\mathbf{U}(z) = \left[\begin{array}{c} \mathbf{v}(z) \\ \hdashline \boldsymbol{\sigma}_z(z) \end{array}\right] = \boldsymbol{\Xi}\ \mathcal{E}(z)\ \mathbf{a}\,,\ -h < z < h\,, \qquad (4)$$

where $\mathbf{v}$ is the velocity vector and $\boldsymbol{\sigma}_z$ the stress in the z-direction. The matrix $\boldsymbol{\Xi} = \left(\begin{array}{c:c:c:c} \boldsymbol{\xi}_1 & \cdots & \boldsymbol{\xi}_6 \end{array}\right)$ contains the six-dimensional polarization vectors. The diagonal matrix $\mathcal{E}(z) = \mathrm{diag}\,[\exp(-\mathrm{i}\,\varsigma_\alpha\,z)]_{1\leqslant\alpha\leqslant 6}$ represents the propagation, $\varsigma_\alpha = \varsigma'_\alpha - \mathrm{i}\,\varsigma''_\alpha$ denoting the slowness in the z-direction. The six pairs $(\varsigma_\alpha\,,\,\boldsymbol{\xi}_\alpha)_{1\leqslant\alpha\leqslant 6}$ are the solutions of the eigenvalue equation $\mathcal{S}\ \boldsymbol{\xi}_\alpha = \varsigma_\alpha\,\boldsymbol{\xi}_\alpha$, where $\mathcal{S}$ is the real-valued Stroh matrix defined in [2]. $(2\,\mathbb{r})$ of them are real and correspond to homogeneous (or bulk) waves. $(3 - \mathbb{r})$ pairs of them are complex conjugate and define *conjugate* inhomogeneous (or surface) waves.

Let us consider the matrix $\mathbb{T}$:

$$\mathbb{T} = \frac{-1}{4}\left(\begin{array}{c:c} \mathbb{O} & \mathbb{I}_3 \\ \hdashline \mathbb{I}_3 & \mathbb{O} \end{array}\right)\,, \qquad (5)$$

$\mathbb{I}_3$ and $\mathbb{O}$ denoting the three-by-three identity matrix and the zero matrix of any dimension, respectively. The matrix $\mathbb{T}$ is taken such that $\boldsymbol{\xi}_\alpha^{\mathrm{T}}\,\mathbb{T}\,\boldsymbol{\xi}_\alpha$ is the third component of the Poynting vector of the α^{th} exponential solution if both the z-component of the slowness and the polarization vectors are real-valued, *i.e.* $\boldsymbol{\xi}_\alpha^{\mathrm{T}}\,\mathbb{T}\,\boldsymbol{\xi}_\alpha$ is the average power flux in the

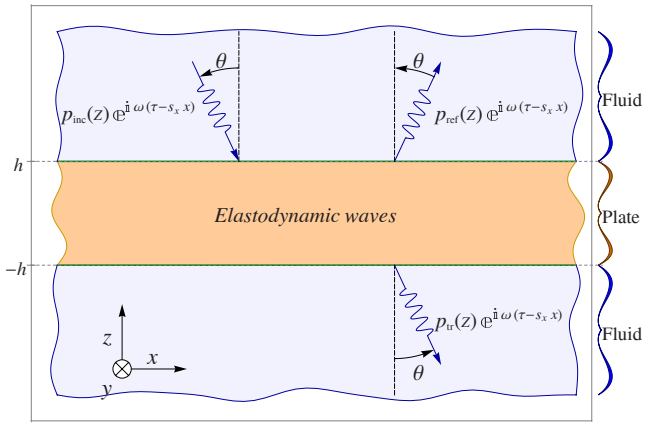

Figure 1: An elastic plate immersed in a fluid, insonified by a plane wave of incidence angle θ.

z-direction for any homogeneous solution (see [2] for more details).

Assuming for simplicity that the six eigenvalues are different, the numbering of the six pairs $(\varsigma_\alpha\,,\,\boldsymbol{\xi}_\alpha)_{1\leqslant\alpha\leqslant 6}$ is made as follows:

$$\begin{array}{llll} \varsigma_\alpha\in\mathbb{R}, & \boldsymbol{\xi}_\alpha\in\mathbb{R}^6 & \boldsymbol{\xi}_\alpha^{\mathrm{T}}\,\mathbb{T}\,\boldsymbol{\xi}_\alpha=1 & 1\leqslant\alpha\leqslant\mathbb{r} \\ \mathit{Im}\,(\varsigma_\alpha)<0 & \mathit{Im}\,(\boldsymbol{\xi}_\alpha)\neq\mathbf{0}_6 & \boldsymbol{\xi}_\alpha^{\mathrm{T}}\,\mathbb{T}\,\boldsymbol{\xi}_\alpha=1 & \mathbb{r}<\alpha\leqslant 3 \\ \varsigma_\alpha\in\mathbb{R}, & \boldsymbol{\xi}_\alpha\in\mathbb{R}^6 & \boldsymbol{\xi}_\alpha^{\mathrm{T}}\,\mathbb{T}\,\boldsymbol{\xi}_\alpha=-1 & 4\leqslant\alpha\leqslant 3+\mathbb{r} \\ \varsigma_\alpha=\varsigma_{\alpha-3}^{*} & \boldsymbol{\xi}_\alpha=\boldsymbol{\xi}_{\alpha-3}^{*} & \boldsymbol{\xi}_\alpha^{\mathrm{T}}\,\mathbb{T}\,\boldsymbol{\xi}_\alpha=1 & 3+\mathbb{r}<\alpha\leqslant 6 \end{array} \tag{6}$$

such that the first three waves are upgoing (positive power flux ϕ_α for bulk waves/decreasing amplitude $\exp(-\omega\,\varsigma_\alpha''\,z)$ with increasing z for surface waves) and the last three waves are downgoing (negative power flux/decreasing amplitude with decreasing z).

2.2.2 Non standard upgoing and downgoing waves

The mean power flux ϕ through any plane z=z_0 is the z-component of the Poynting vector which can be expressed with respect to the components a_α of the vector $\mathbf{a}$ [Eq. (4)]. Because this flux, espressed as follows:

$$\phi=\sum_{\alpha=1}^{\mathbb{r}}\left|a_\alpha\right|^2-\sum_{\alpha=4}^{3+\mathbb{r}}\left|a_\alpha\right|^2+\sum_{\alpha=\mathbb{r}+1}^{3}a_\alpha\,a_{\alpha+3}^{*}+a_\alpha^{*}\,a_{\alpha+3}\,, \tag{7}$$

contains interaction terms $(a_\alpha\,a_{\alpha+3}^{*}+a_\alpha^{*}\,a_{\alpha+3})$ for inhomogeneous components, *nonstandard upgoing and downgoing waves* are respectively defined as follows:

$$\tilde{\mathbf{N}}_\alpha(z)=\frac{1}{\sqrt{2}}\left[\mathrm{e}^{-\mathrm{i}\,\varsigma_\alpha\,(Z-Z_\alpha)}\,\boldsymbol{\xi}_\alpha+\mathrm{e}^{-\mathrm{i}\,\varsigma_\alpha^{*}\,(Z-Z_\alpha)}\,\boldsymbol{\xi}_\alpha^{*}\right], \tag{8}$$

$$\tilde{\mathbf{N}}_{\alpha+3}(z)=\frac{1}{\sqrt{2}}\left[-\mathrm{e}^{-\mathrm{i}\,\varsigma_\alpha\,(Z-Z_\alpha)}\,\boldsymbol{\xi}_\alpha+\mathrm{e}^{-\mathrm{i}\,\varsigma_\alpha^{*}\,(Z-Z_\alpha)}\,\boldsymbol{\xi}_\alpha^{*}\right], \tag{9}$$

where the origin z_α of the z-axis can be chosen arbitrarily, for any α such that $\mathbb{r}$<α⩽3. Due to the symmetry of the problem, the origins z_α are taken equal to zero in the present paper (for more details on this point, see [2]). An example of waveform is drawn in Fig. 2 in the case where the real part of ς_α is zero. For homogeneous waves, *i.e.* $1\leqslant\alpha\leqslant\mathbb{r}$ or $4\leqslant\alpha\leqslant 3+\mathbb{r}$, $\tilde{\mathbf{N}}_\alpha(z)=\mathrm{e}^{-\mathrm{i}\,\varsigma_\alpha\,Z}\,\boldsymbol{\xi}_\alpha$.

Indeed the mean power flux ϕ associated to the six-dimensional vector $\mathbf{U}(z)=\tilde{N}(z)\,\tilde{\mathbf{a}}$, where the matrix $\tilde{N}$ is $\left(\tilde{\mathbf{N}}_1\,\vdots\cdots\vdots\,\tilde{\mathbf{N}}_6\right)$, becomes:

$$\phi=\sum_{\alpha=1}^{3}\left|\tilde{a}_\alpha\right|^2-\sum_{\alpha=4}^{6}\left|\tilde{a}_\alpha\right|^2\,. \tag{10}$$

This flux is the sum of the fluxes of three upgoing waves minus the sum of the fluxes of three downgoing waves, without any interaction term.

Linearity and energy conservation imply that $\tilde{\mathbf{a}}$=$\tilde{\mathbf{g}}\,a_{\mathrm{inc}}$ and:

$$1-|r|^2=-\sum_{\alpha=1}^{3}\left|\tilde{g}_\alpha\right|^2+\sum_{\alpha=4}^{6}\left|\tilde{g}_\alpha\right|^2=|t|^2\,. \tag{11}$$

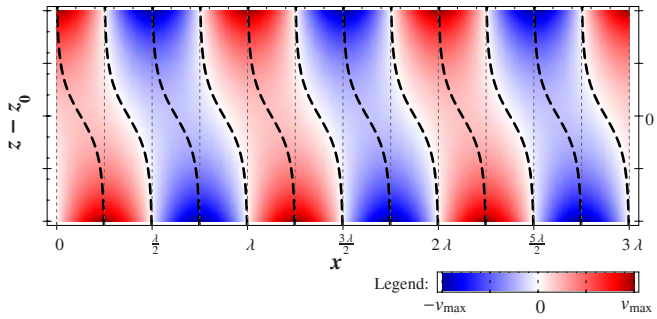

Figure 2: Magnitude of non-zero coordinates of nonstandard progressive waves in the case where the slowness ς_α is purely imaginary.

2.3 Debye series

2.3.1 The first reflection/transmission

The downgoing incident acoustic wave, in the fluid above the plate, produces an upgoing reflected wave, with a reflection coefficient $\tilde{r}_0$, and a transmitted downgoing elastic wave, with a transmission vector $\tilde{\mathbf{g}}_0$, such that:

$$\mathbb{K}\,\tilde{N}(H)\begin{pmatrix}\mathbf{0}\\ \hdashline \tilde{\mathbf{g}}_0\end{pmatrix}-\tilde{r}_0\,\mathbf{h}_{\mathrm{up}}=\mathbf{h}_{\mathrm{down}}, \tag{12}$$

the four-by-six matrix $\mathbb{K}$ being $\left(\mathbb{O}\,\vdots\,\mathbb{I}_4\right)$ and the four-dimensional vectors $\mathbf{h}_{\mathrm{up,down}}$ being $\left(\pm\sqrt{2\,s_z/\rho}\;\;0\;\;0\;\;-\sqrt{2\rho/s_z}\right)^{\mathrm{T}}$.

2.3.2 Internal reflections/transmissions

In the plate, each downgoing elastic wave produces at the lower interface an upgoing reflected elastic wave, with a reflection matrix $\tilde{\mathcal{R}}_{\mathrm{bot}}$, and a transmitted downgoing acoustic wave, with a tranmission vector $\tilde{\mathbf{t}}_{\mathrm{bot}}$, such that:

$$\mathbb{K}\,\tilde{N}(-H)\begin{pmatrix}\tilde{\mathcal{R}}_{\mathrm{bot}}\\ \hdashline \mathbb{I}_3\end{pmatrix}-\mathbf{h}_{\mathrm{down}}\,\tilde{\mathbf{t}}_{\mathrm{bot}}^{\mathrm{T}}=\mathbf{0}\,. \tag{13}$$

Similarly, at the upper interface:

$$\mathbb{K}\,\tilde{N}(H)\begin{pmatrix}\mathbb{I}_3\\ \hdashline \tilde{\mathcal{R}}_{\mathrm{top}}\end{pmatrix}-\mathbf{h}_{\mathrm{up}}\,\tilde{\mathbf{t}}_{\mathrm{top}}^{\mathrm{T}}=\mathbf{0}\,. \tag{14}$$

The successive reflections/transmissions are represented in Fig. 3.

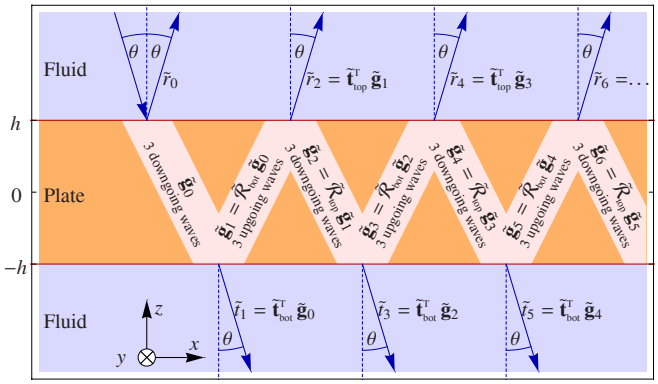

Figure 3: Successive reflections/refractions in an immersed plate.

2.3.3 Global coefficients

The global fields result from successive reflections/transmissions. The vector $\tilde{\mathbf{g}}$ characterizing the vibration of the plate satisfies [2]:

$$\tilde{\mathbf{g}} = \left[\sum_{n}^{+\infty}\begin{pmatrix}\mathbb{O} & \tilde{\mathcal{R}}_{\mathrm{bot}}\\ \tilde{\mathcal{R}}_{\mathrm{top}} & \mathbb{O}\end{pmatrix}^2\right]\begin{pmatrix}\mathbf{0}\\ \tilde{\mathbf{g}}_0\end{pmatrix} = \begin{pmatrix}\tilde{\mathcal{R}}_{\mathrm{bot}}\,\tilde{\mathbf{g}}_{\mathrm{down}}\\ \tilde{\mathbf{g}}_{\mathrm{down}}\end{pmatrix}, \qquad (15)$$

where the three-dimensional vector

$$\tilde{\mathbf{g}}_{\mathrm{down}} = \left[\sum_{n}^{+\infty}\left(\tilde{\mathcal{R}}_{\mathrm{top}}\,\tilde{\mathcal{R}}_{\mathrm{bot}}\right)^n\right]\tilde{\mathbf{g}}_0 = \left(\mathbb{I}_3 - \tilde{\mathcal{R}}_{\mathrm{top}}\,\tilde{\mathcal{R}}_{\mathrm{bot}}\right)^{-1}\tilde{\mathbf{g}}_0 \qquad (16)$$

is the product of the sum of the so-called Debye series by the vector $\tilde{\mathbf{g}}_0$.

The reflection and transmission coefficients are:

$$r = \tilde{r}_0 + \tilde{\mathbf{t}}^{\mathrm{T}}_{\mathrm{top}}\,\tilde{\mathcal{R}}_{\mathrm{bot}}\,\tilde{\mathbf{g}}_{\mathrm{down}}\,, \quad t = \tilde{\mathbf{t}}^{\mathrm{T}}_{\mathrm{bot}}\,\tilde{\mathbf{g}}_{\mathrm{down}}\,. \qquad (17)$$

From Eqs. (12-17), it is obvious that the vector $\tilde{\mathbf{g}}$ and the coefficients r and t satisfy the boundary conditions:

$$\mathbb{K}\,\tilde{\mathcal{N}}(H)\,\tilde{\mathbf{g}} - r\,\mathbf{h}_{\mathrm{up}} = \mathbf{h}_{\mathrm{down}}\,, \quad \mathbb{K}\,\tilde{\mathcal{N}}(-H)\,\tilde{\mathbf{g}} - t\,\mathbf{h}_{\mathrm{down}} = \mathbf{0}\,. \qquad (18)$$

(a)

Aluminium		
$\rho_0 = 2700\,kg{\cdot}m^{-3}$	$c_{\mathrm{L}} = 6420\,m{\cdot}s^{-1}$	$c_{\mathrm{T}} = 3040\,m{\cdot}s^{-1}$

Water	
$\rho = 1000\,kg{\cdot}m^{-3}$	$c = 1550\,m{\cdot}s^{-1}$

(b)

	Longitudinal	Transverse	Rayleigh
Adimensional slownesses	$\frac{c_{\mathrm{T}}}{c_{\mathrm{L}}}\approx 0.474$	$\frac{c_{\mathrm{T}}}{c_{\mathrm{T}}}=1$	$\frac{c_{\mathrm{T}}}{c_{\mathrm{R}}}\approx 1.069$
Critical angles	$\theta_{\mathrm{L}}\approx 13.97^\circ$	$\theta_{\mathrm{T}}\approx 30.66^\circ$	$\theta_{\mathrm{R}}\approx 33.01^\circ$

Table 1: Numerical values for aluminium and water: (a) velocities and densities; (b) dimensionless slownesses and critical angles.

2.4 Lamb waves

Both total transmission and zero reflection can be associated to Lamb wave generation, which are obtained for complex frequencies [4], as shown on Fig. 4 for an aluminium plate immersed in water (Tab. 1), where the 3D graph represents the transmission coefficient versus the angle of incidence and the frequency-thickness product. On this image, the dispersion curves of complex frequency Lamb waves are plotted as well (dashed lines).

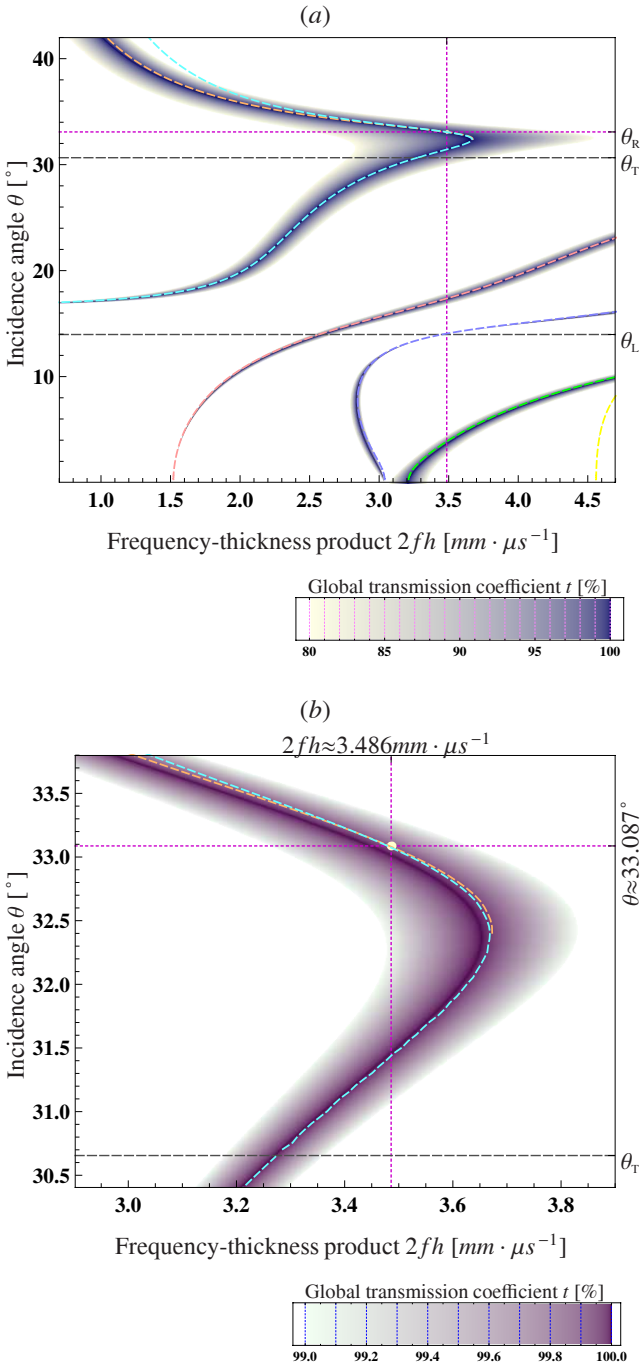

Figure 4: Global transmission coefficient t for an aluminium plate immersed in water, with respect to the frequency-thickness product and the angle of incidence.

For these particular conditions, the interferences within the plate between the upgoing and downgoing waves are of a maximum intensity for Lamb waves, as illustrated on Fig. 5, where the frequency-thickness product is near $3.486 mm{\cdot}\mu s^{-1}$. On this figure, the total energy associated with the reflected ($|r|^2$), transmitted ($|t|^2$), upgoing ($|\tilde{\mathbf{g}}_{\mathrm{up}}|^2$) and downgoing ($|\tilde{\mathbf{g}}_{\mathrm{down}}|^2$) waves are plotted versus the angle of incidence. For the S_2, A_1 and S_0 modes, the upgoing and downgoing energies are both very large. This reveals the existence of strong interferences in the plate, which is the intrinsic nature

of guided waves. Such interpretation would not be possible by using the classical inhomogenous waves in the plate.

This behaviour is general for any points on the dispersion curves, except close to the Rayleigh angle θ_R (see Fig. 5). Let us examine in detail in the next section this unique area where a Lamb wave can be generated at the Rayleigh angle (see Fig. 4b).

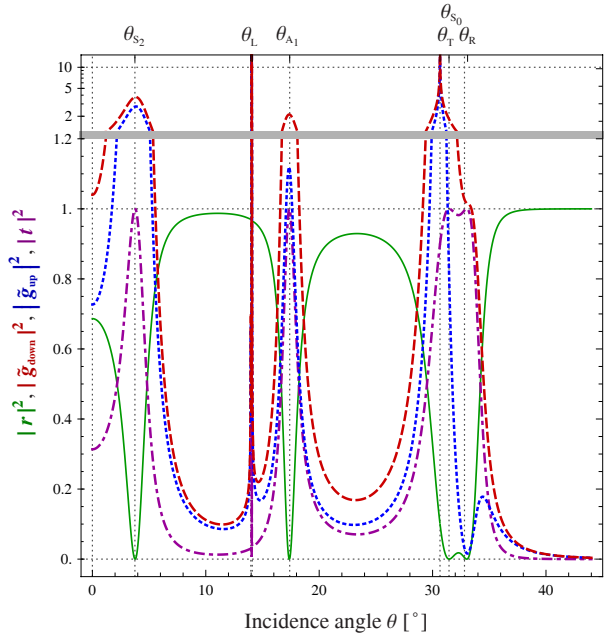

Figure 5: Global coefficients: $|r|^2$ (reflection, solid), $|t|^2$ (transmission, dash-dot), $|\tilde{\mathbf{g}}_{up}|^2$ (upgoing energy, dotted) and $|\tilde{\mathbf{g}}_{down}|^2$ (downgoing energy, dashed) for the frequency-thickness product $2fh \approx 3.486 mm \cdot \mu s^{-1}$.

3 First reflections for isotropic plates

We focus in this section firstly on the first reflection/refraction at the upper interface, characterized by the reflection coefficient $\tilde{r}_0$ and the vector $\tilde{\mathbf{g}}_0$, and lastly on the second reflection/refraction at the lower interface, with the transmission coefficient $\tilde{t}_1 = \tilde{\mathbf{t}}_{bot}^T \tilde{\mathbf{g}}_0$ (see Fig.3).

Only the case of isotropic plates is considered such that analytical calculations can be performed. An isotropic elastic material is characterized by the longitudinal and transverse velocities c_L and c_T, and the density ρ_0. The two critical angles $\theta_{L,T}$ satisfy $\sin\theta_{L,T} = c / c_{L,T}$. The numerical values for an aluminium plate immersed in water are given in Table 1.

3.1 Impedance matching at the upper interface

The first reflection coefficient $\tilde{r}_0$ can be expressed as follows:

$$\begin{cases} \dfrac{\mathbb{l}-\mathbb{m}+\mathbb{i}\,\mathbb{n}}{\mathbb{l}-\mathbb{m}-\mathbb{i}\,\mathbb{n}} & , \ \theta < \theta_L \,, \\ \dfrac{\mathbb{l}-(\mathbb{i}\,\mathbb{m}+\mathbb{n})\,\mathbb{X}-\mathbb{i}\,(\mathbb{l}\,\mathbb{X}-\mathbb{i}\,\mathbb{m}+\mathbb{n})}{\mathbb{l}-(\mathbb{i}\,\mathbb{m}-\mathbb{n})\,\mathbb{X}-\mathbb{i}\,(\mathbb{l}\,\mathbb{X}-\mathbb{i}\,\mathbb{m}-\mathbb{n})} & , \ \theta_L < \theta < \theta_T \,, \\ \dfrac{(\mathbb{l}-\mathbb{m})(\mathbb{X}\mathbb{Y}-1)+\mathbb{n}\,(\mathbb{X}-\mathbb{Y})+\mathbb{i}\,[(\mathbb{l}+\mathbb{m})(\mathbb{X}+\mathbb{Y})-\mathbb{n}\,(\mathbb{X}\mathbb{Y}+1)]}{(\mathbb{l}-\mathbb{m})(\mathbb{X}\mathbb{Y}-1)-\mathbb{n}\,(\mathbb{X}-\mathbb{Y})+\mathbb{i}\,[(\mathbb{l}+\mathbb{m})(\mathbb{X}+\mathbb{Y})+\mathbb{n}\,(\mathbb{X}\mathbb{Y}+1)]} & , \ \theta_T < \theta \,, \end{cases} \tag{19}$$

where $\mathbb{l}=(2\beta^2-1)^2$, $\mathbb{m}=-4\beta^2\beta_L\beta_T$ and $\mathbb{n}=\mathbb{i}\,\rho\beta_L/(\rho_0\beta_F)$ are dimensionless coefficients. The values $\mathbb{X}$ and $\mathbb{Y}$ are equal to $\exp\left(-2\,\mathbb{i}\,\beta_{L,T}\,\omega h / c_{L,T}\right)$, respectively, h being the distance between the interface and the z-origins of the nonstandard inhomogeneous waves. These values are both real after the second critical angle ($\theta > \theta_T$). $\beta = c_T \sin\theta / c$, $\beta_F = \sqrt{c_T^2\, c^{-2} - \beta^2}$, $\beta_{L,T} = \sqrt{c_T^2\, c_{L,T}^{-2} - \beta^2}$ or $-\mathbb{i}\sqrt{\beta^2 - c_T^2\, c_{L,T}^{-2}}$.

Before the first critical angle ($\theta < \theta_L$), impedance matching can occur, *i.e.* the reflection coefficient $\tilde{r}_0$ can be equal to zero, if the density ratio (ρ / ρ_0) is high enough such that it can be equal to $\beta_F^{-1}\beta_L(\mathbb{l}-\mathbb{m})$. For an aluminium plate immersed in water, the density ratio is too low (see Fig. 6). Note that in this case, only homogeneous waves are involved and consequently the reflection coefficient is the same for each choice of downgoing inhomogeneous elastic waves.

Between the two critical angles, one can demonstrate that the reflection coefficient $\tilde{r}_0$ can not be equal to zero. It can be observed in Fig. 6 that the absolute value of this coefficient is not very sensible to the frequency-distance product ($f\,h$).

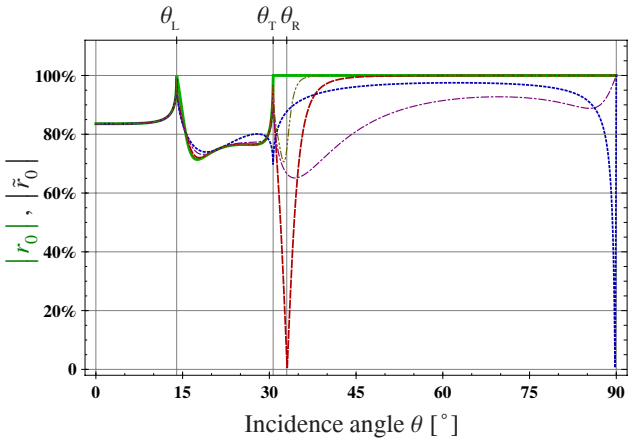

Figure 6: The absolute value of the first reflection coefficient in the standard exponential basis (solid) and in the nonstandard basis for an aluminium plate immersed in water, the frequency-distance product ($f\,h$) having the following values: 0 (dotted), $0.7 mm \cdot \mu s^{-1}$ (–·), $1.743 mm \cdot \mu s^{-1}$ (dashed) and $3.0 mm \cdot \mu s^{-1}$ (–··).

On the contrary, when the longitudinal and transverse waves are both inhomogeneous ($\theta > \theta_T$), the absolute value of this coefficient is sensible to the frequency-distance product ($f\,h$). Indeed, one can demonstrate that a necessary and sufficient condition of existence of a pair $(\mathbb{X}, \mathbb{Y})$ such that $\tilde{r}_0 = 0$ [Eq. (19)] is:

$$-\mathbb{n}^2 \leqslant \mathbb{l}^2 - \mathbb{m}^2 \leqslant \mathbb{n}^2 \quad \text{and} \quad \mathbb{l} + \mathbb{m} \geqslant \mathbb{n} \,. \tag{20}$$

The coefficients $\mathbb{X}$ and $\mathbb{Y}$ are then expressed as follows:

$$\begin{aligned} \mathbb{X} &= \frac{2\,\mathbb{l}\,\mathbb{n} \pm \sqrt{[(\mathbb{l}+\mathbb{m})^2 - \mathbb{n}^2]\,[\mathbb{n}^2 - (\mathbb{l}-\mathbb{m})^2]}}{\mathbb{n}^2 - (\mathbb{m}^2 - \mathbb{l}^2)} \,, \\ \mathbb{Y} &= \frac{2\,\mathbb{m}\,\mathbb{n} \pm \sqrt{[(\mathbb{l}+\mathbb{m})^2 - \mathbb{n}^2]\,[\mathbb{n}^2 - (\mathbb{l}-\mathbb{m})^2]}}{\mathbb{n}^2 - (\mathbb{l}^2 - \mathbb{m}^2)} \,. \end{aligned} \tag{21}$$

Note that $\mathbb{l}^2 - \mathbb{m}^2 = \left(2\beta^2 - 1\right)^4 - \left[4\beta^2\,(\mathbb{i}\beta_L)(\mathbb{i}\beta_T)\right]^2$ is the Rayleigh polynomial and that the solution of $\mathbb{l} = \mathbb{m}$ corresponds to the Rayleigh wave (in vaccum).

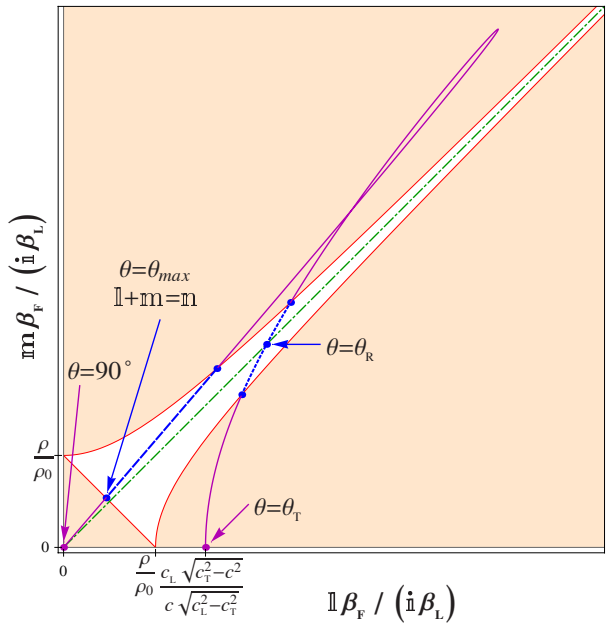

Figure 7: The parametric curve of $\beta_F\,(\mathbb{i}\beta_L)^{-1}$ ($\mathbb{I}$, $\mathbb{m}$) as a function of the incidence angle θ. The white zone corresponds to Condition (20) of existence of impedance matching.

Provided that the sound velocity in the fluid is lower than the velocity of the Rayleigh wave and that the density ratio ($\rho\,/\,\rho_0$) is not too high, we can observe on Fig. 7 that impedance matching can occur if the incidence angle is either in an interval (dotted line) around θ_R, the angle for which the Rayleigh wave is excited, or in another interval (dashed line) with upper bound θ_{max} just lower than 90°. The lower is the density ratio, the narrower are these intervals. In each interval, only one value of the frequency-distance product ($f\,h$) can be found such that Eq. (21) is satisfied. The first one corresponds to an incidence angle near θ_R. For example, for an aluminium plate immersed in water [2], $\theta\approx33.087^\circ$ and $(f\,h)\approx1.743 mm\cdot\mu s^{-1}$ (see also Fig. 6). The second one corresponds to the incidence angle θ_{max}, such that $\mathbb{I}+\mathbb{m}=\mathbb{n}$, and h=0 ($\mathbb{X}=\mathbb{Y}=1$).

3.2 First transmission at the lower interface

Let us now consider the transmission coefficient $\tilde{t}_1$ at the lower interface, for an angle of incidence greater than the second critical angle. This lower interface receives two non-standard inhomogeneous waves generated at the upper interface: a P-wave, characterized by the component $\tilde{g}_{0\,P}$ of the vector $\tilde{\mathbf{g}}_0$, and a SV-wave, with the component $\tilde{g}_{0\,SV}$. The SH-component is zero because a SH-wave cannot be generated from the fluid. These components are expressed as follows:

$$\tilde{g}_{0\,P} = \frac{2\,(1-\mathbb{i})(Y+\mathbb{i})\,\sqrt{\mathbb{I}\,\mathbb{n}\,X}}{\text{<denominator of } \tilde{r}_0\text{, } Eq.\ (19.3)>}\,, \tag{22}$$

$$\tilde{g}_{0\,SV} = \frac{-2\,(1+\mathbb{i})(X-\mathbb{i})\,\sqrt{\mathbb{m}\,\mathbb{n}\,Y}}{\text{<denominator of } \tilde{r}_0\text{, } Eq.\ (19.3)>}\,, \tag{23}$$

and satisfy $\left|\tilde{g}_{0\,P}^2\right|+\left|\tilde{g}_{0\,SV}^2\right|=1-\left|\tilde{r}_0^2\right|$ (energy conservation).

Due to both the symmetry with respect to z=0 and reciprocity, the transmission vector $\tilde{\mathbf{t}}_{bot}$ at the lower interface satisfies $\tilde{\mathbf{t}}_{bot}=-\tilde{\mathbf{g}}_0$ [2]. Consequently, the transmission coefficient $\tilde{t}_1$ is equal to $-\tilde{g}_{0\,P}^2-\tilde{g}_{0\,SV}^2$. Thus, if there is a perfect impedance matching at the upper interface, the energy will be fully transmitted without any reflection provided than the phases of $\tilde{g}_{0\,P}^2$ and $\tilde{g}_{0\,SV}^2$ are identical, *i.e.* the phases of $(1+\mathbb{i}\,X)^2$ and $(Y+\mathbb{i})^2$ are the same. Unfortunately, this is not exactly possible because both X and Y are reals between zero and one for a (non-zero) plate thickness $2h$.

However, in the case of an aluminium plate immersed in water, a frequency-thickness product $(2\,f\,h)\approx3.486 mm\cdot\mu s^{-1}$ and an incidence angle of 33.087° yield to a direct transmission coefficient $\tilde{t}_1$ of absolute value near 97.0% and to a global transmission coefficient t of absolute value near 99.95% (see Fig. 4b).

4 Conclusion

In the case of incidence angles associated to Lamb waves, total transmission and zero reflection are the result of large interferences between the successive reflections/refractions in the plate. In this latter case, the energy is progressively released by the plate to the fluid by successive transmissions with weak amplitudes. Up to now, the explanation of Lamb wave generation by constructive interferences in the plate held true only when no evanescent plane wave participates to this multiple reflections. With the new definition of upgoing and downgoing waves, introduced in this paper, this description is extended to any angle of incidence. An exception is however observed. Indeed, at the incidence angle close to that associated to the Rayleigh wave, the incident wave in the upper fluid is totally transmitted to the lower fluid, without any multiple reflection/refraction in the plate. In this latter case, the plate seems to be really transparent.

References

[1] P. Chadwick, G. D. Smith, "Foundations of the theory of surface waves in anisotropic elastic materials", *Advances in Applied Mechanics* **17**, 303-376 (1977).

[2] E. Ducasse, M. Deschamps, "A nonstandard wave decomposition to ensure the convergence of Debye series for modeling wave propagation in an immersed anisotropic elastic plate", *Wave Motion*, under revision.

[3] J. Lothe, D. M. Barnett, "On the existence of surface-wave solutions for anisotropic elastic half-spaces with free surface", *J. Applied Physics* **704**(2), 428-433 (1976).

[4] O. Poncelet, M. Deschamps, "Lamb waves generated by complex harmonic inhomogeneous plane waves", *J. Acoust. Soc. Am.* **102**(1), 292-300 (1997).

[5] A. L. Shuvalov, O. Poncelet, M. Deschamps, "Analysis of the dispersion spectrum of fluid-loaded anisotropic plates: flexural- type branches and real-valued loops", *J. Sound Vib.* **290**, 1175-1201 (2006).

[6] A. N. Stroh, Steady state problems in anisotropic elasticity, J. Math. and Physics 41 (1962) 77-103.

[7] T. C. T. Ting, *Anisotropic Elasticity*, Oxford University Press, Oxford (1996), ISBN 978-0195074475.